

www.acsami.org Research Article

Photonic Lift-off Process to Fabricate Ultrathin Flexible Solar Cells

Wen Liu, Vikram S. Turkani, Vahid Akhavan, and Brian A. Korgel*



Cite This: https://doi.org/10.1021/acsami.1c12382



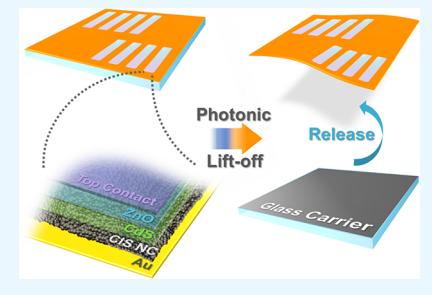
ACCESS

III Metrics & More



SI Supporting Information

ABSTRACT: A microsecond time-scale photonic lift-off (PLO) process was used to fabricate mechanically flexible photovoltaic devices (PVs) with a total thickness of less than 20 μ m. PLO is a rapid, scalable photothermal technique for processing extremely thin, mechanically flexible electronic and optoelectronic devices. PLO is also compatible with large-area devices, roll-to-roll processing, and substrates with low temperature compatibility. As a proof of concept, PVs were fabricated using CuInSe₂ nanocrystal ink deposited at room temperature under ambient conditions on thin, plastic substrates heated to 100 °C. It was necessary to prevent cracking of the brittle top contact layer of indium tin oxide (ITO) during lift-off, either by using a layer of silver nanowires (AgNW) as the top contact or by infusing the ITO layer with AgNW. This approach could generally be



used to improve the mechanical versatility of current collectors in a variety of ultrathin electronic and optoelectronic devices requiring a transparent conductive contact layer.

KEYWORDS: photonic lift-off, ultrathin photovoltaics, flexible devices, copper indium diselenide (CuInSe₂), nanocrystals, solution-processable, transparent conducting electrodes, top contact

■ INTRODUCTION

There are many emerging applications for flexible, lightweight photovoltaic devices (PVs) such as building and product-integrated designs that are easy to install with effective solar energy-harvesting capability. Bendable and foldable PVs are particularly well-suited for application on nonflat surfaces. Human-centered personal applications such as smart home "Internet-of-Things" systems and wearable electronic devices also benefit from thin PVs with atypical form factors. Jeghtweight, flexible PVs offer the potential for high-throughput roll-to-roll production with lower thermal budget and reduced substrate material costs. 5–7

Fabrication processes for electronic and optoelectronic semiconductor devices, however, have generally been developed based on the use and handling of rigid substrates. For example, PVs are usually made on bulky wafers or thick pieces of glass. Mechanically flexible, lightweight solar cells typically require significant changes in manufacturing approaches. Plastic substrates cannot tolerate high temperature processing, and extremely thin (<20 μ m) devices are too fragile to handle. In this context, lift-off techniques offer a useful approach to device fabrication, requiring only minimal adjustments to well-optimized processes.

In a lift-off process, active device structures are fabricated on a rigid carrier substrate and then removed using either physical, chemical, or thermal methods. Physical methods of cleavage rely on the exertion of significant mechanical forces, which can crack the devices and make achieving process uniformity a challenge. 8–13 Chemically aided lift-off involves the dissolution of sacrificial layers between the device and the substrate, often relying on corrosive etchants that can damage device

components. 14-17 This demands new materials and device designs to avoid a loss of essential device function. Lift-off methods using localized heating with a laser have become attractive.¹⁸ However, beam-width limitations pose a challenge to process throughput.¹⁹ Another problem is that excimer lasers operating with ultraviolet (UV) wavelength lead to ashing of organic and polymer materials due to their strong light absorption.²⁰ A different light-driven thermal approach called photonic lift-off (PLO) uses the photothermal response of a metal-coated glass substrate to promote the release of a device layer illuminated with high-intensity pulsed light. The temperature at the point of light absorption can get very hot, with temperatures reaching up to 855 °C, but with light pulses lasting less than 200 μ s, it can be used to detach devices without damage since the localized heating is rapidly dissipated through the supporting substrate. In contrast to laser lift-off, direct illumination of the polymer is prevented by the metal layer, which prevents ashing and provides for a clean lift-off process. The power density and duration of the light pulses are widely tunable, making the use of PLO on a wide variety of heat-sensitive films and materials, including polymeric substrates, possible. PLO also offers large illumination areas, making rapid processing of large area substrates and roll-to-roll scalability possible.

Received: July 1, 2021



Here, we demonstrate the use of the PLO technique to produce ultrathin PVs less than 20 µm thick using a commercially available photonic curing tool (PulseForge Invent Model IX2-951, NovaCentrix). PV devices were fabricated on polyimide (PI) films using a CuInSe2 nanocrystal ink as the semiconductor light-absorber layer. This nanocrystal ink enables working devices to be made without high-vacuum deposition or high-temperature (>550 °C) selenium vapor annealing of the CuInSe₂ layer. CuInSe₂ nanocrystals are stable in air and can be conveniently deposited by spray coating under ambient conditions (<100 °C) without further sintering at elevated temperatures. Other kinds of nanocrystals, such as metal halide perovskites, PbS, PbSe, or CdTe, can be used to make PVs as well, but they are processed under inert environmental conditions. 21-24 We found that the typical top contact layer of indium tin-oxide (ITO) was prone to cracking during the lift-off process and significantly limited the mechanical flexibility of the devices. To overcome this, a top contact of silver nanowires (AgNW) or a mixed layer of ITO and AgNW was found to significantly improve the durability of the devices and enable damage-free lift-off of the devices.

■ EXPERIMENTAL METHODS

Materials. Copper(I) chloride (CuCl, anhydrous, >99.99%), indium(III) chloride (InCl₃, anhydrous, ≥99.999%), elemental selenium (Se, 99.99%), oleylamine (OLAm, technical grade 70%), tributylphosphine (TBP, 97%), diphenylphosphine (DPP, 98%), toluene (anhydrous, 99.8%), cadmium sulfate (CdSO₄, ≥99.99%), and thiourea $((NH_2)_2CS, \geq 99\%)$ were obtained from MilliporeSigma. Toluene (ACS reagent, ≥99.5%), ethanol (anhydrous, ACS/USP grade), and ammonium hydroxide (NH₄OH, 18 M) were purchased from Fisher Scientific. Ultrapure (type I) grade deionized water (DI- H_2O) was used with a resistivity of 18.2 M Ω -cm at 25 °C. Polished soda-lime glass (25 × 25 × 1.1 mm) was purchased from Delta Technologies. The rigid carriers used in the PLO process were obtained from Thin Film Devices, USA. These substrates were composed of 500 µm-thick Eagle XG slim glass substrates (Corning, USA) with 200 nm of W/Ti alloy (80:20) sputtered on one side as the light-absorber layer (LAL). A PI2525 polyimide (PI) precursor solution was purchased from HD MicroSystems. AgNW dispersed in isopropanol at a concentration of 20 mg/mL were purchased from ACS Material. OLAm was stored in a N₂-filled glovebox prior to use after degassing on a Schlenk line at 110 °C under vacuum for 1 h followed by blanketing with N2 overnight at 110 °C. All other materials were used as received.

CulnSe₂ Nanocrystal Synthesis. Colloidal ligand-stabilized CuInSe₂ nanocrystals were synthesized by a combination of heat-up and hot injection using two different phosphine precursors. TBP:Se was used as the Se source, and DPP was added to increase the reaction yield. 4,25,26 A solution of TBP:Se was prepared in a N₂-filled glovebox by dissolving Se powder (0.790 g, 10 mmol) in 10 mL of TBP at room temperature. Also in a N2-filled glovebox, a reactant solution of 50 mL of OLAm, CuCl (0.495 g, 5 mmol), InCl₃ (1.106 g, 5 mmol), and 1.5 mL DPP was prepared in a 125 mL three-neck flask. The three-neck flask was sealed by septa and wires and transferred to a Schlenk line. The mixture was placed under vacuum for 30 min at 110 °C and then blanketed with N_2 at 110 °C for another 10 min. The mixture was heated to 180 $^{\circ}$ C at a rate of 8 $^{\circ}$ C min⁻¹. The TBP:Se precursor solution was then removed from the glovebox with a syringe and rapidly injected into the flask. The temperature was raised to 240 °C at 8 °C min⁻¹. After heating for 10 min at 240 °C, the flask was removed from the heating mantle and allowed to cool to about 50 °C before opening in air to extract the nanocrystal product.

 $\rm CuInSe_2$ nanocrystals were isolated from the crude reaction mixture by precipitation with 20 mL of ethanol and centrifugation at 4500 rpm (2600g for rcf, g being gravity) for 10 min. The slightly black supernatant was discarded. The nanocrystals were redispersed in 6 mL

of toluene and then precipitated again by adding 6 mL of ethanol. After centrifugation at 4500 rpm for 10 min, the supernatant was discarded. The nanocrystals were redispersed in a minimal amount of toluene (\sim 7 mL) and transferred to a 20 mL glass vial. The nanocrystals were dried, transferred into a N₂-filled glovebox, and then redispersed in anhydrous toluene to obtain a concentration of 100 mg mL⁻¹. Typical reactions yield 650 mg of nanocrystal product.

Solar Cell Fabrication and Testing. $1'' \times 1''$ LAL-coated glass substrates were used as the rigid carrier to support PI film preparation and deposition of the PV device layers shown in Figure 1. About 0.3

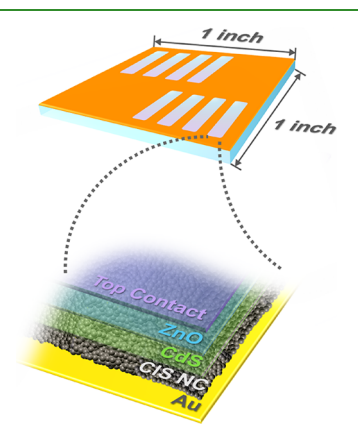


Figure 1. Illustration of the $CuInSe_2$ nanocrystal (CIS NC) solar cell design. The Au bottom contact is deposited on the PI film. The top contact was either ITO, AgNW, or a mixture of ITO and AgNW.

mL of PI2525 polyimide precursor solution was dropped onto the LAL side of each substrate and then spin-coated using a two-step process (500 rpm for 10 s followed by 1000 rpm for 30 s, at an acceleration of 500 rpm s⁻¹). The films were soft-baked to remove the solvent from the coating by stepped heating in air for 10 min at 60 °C, 10 min at 70 $^{\circ}\text{C}$, and then 20 min at 80 $^{\circ}\text{C}$. The dried films were then subjected to a hard-bake at 300 °C for 1 h under N2 to obtain cured PI films with a thickness of 18 μ m. Chromium (10 nm) and gold (80 nm) layers were deposited by thermal evaporation in a Kurt J. Lesker Nano36 thermal deposition system through a patterned mask.²⁷ Using a Sonotek ExactaCoat ultrasonic automated spray system equipped with a 120 kHz ultrasonic nozzle, CuInSe₂ nanocrystals dispersed in toluene at a concentration of 5 mg/mL were spray-deposited onto substrates heated to 100 $^{\circ}$ C. The spray nozzle was raster-scanned across the substrates with a 3 mm raster spacing, at a speed of 10 mm/s, an ink injection rate of 0.1 mL/min, an air pressure of 1.6 psi, and a nozzle-to-substrate height of 11.5 cm. The CdS device layer was deposited onto the nanocrystal films by chemical bath deposition (CBD).²⁸ Aqueous solutions of 160 μ L of 15 mM CdSO₄, 275 μ L of 1.5 M thiourea, and 350 µL of 18 M NH₄OH were mixed and dropped onto substrates heated to 90 °C. The substrates were covered with a glass dish for 2 min, then rinsed with DI-H2O, and dried with compressed N2. Layers of intrinsic ZnO (i-ZnO) and ITO were deposited by radio frequency (RF) sputtering in an Ar atmosphere using a Kurt J. Lesker PVD75 thin film deposition system, with ZnO (99.9%) and ITO (In₂O₃:SnO₂ 9:1, 99.99%) targets supplied by Kurt J. Lesker. The sputter deposition area was shadow-masked into eight rectangular regions corresponding to eight individual devices fabricated on the $1'' \times 1''$ substrate. The active device area varied slightly from 0.08 to 0.11 cm² and was measured in each case to determine all reported power conversion efficiencies (PCE). AgNW were deposited on top contact layers by spray coating under ambient conditions onto the ZnO layer. The AgNW ink was diluted with isopropanol to a concentration of 0.8 mg/mL and deposited with a Sonotek ExactaCoat ultrasonic automated spray system equipped with a 120 kHz ultrasonic nozzle. Typical deposition conditions were a raster spacing of 3 mm, a speed of 10 mm/s, an ink injection rate of 0.1 mL/min, an air pressure of 1.6 psi, and a nozzleto-substrate height of 11.5 cm. The thickness of the AgNW layer was controlled by using either 12, 15, or 18 coating cycles. Eighteen coating cycles yield a 320 nm film thickness. Control devices were made using the same PV device fabrication processes on soda-lime glass instead of PI. For these devices, the glass substrates were cleaned before depositing the Cr and Au layers by placing them in an ultrasonic bath of 1:1 vol % acetone:isopropanol for 5 min followed by 5 min sonication in DI-H₂O and drying with compressed air.

PLO Processing. PLO processing was carried out using a high instantaneous power photonic lift-off tool (PulseForge Invent (IX2-95X)) from NovaCentrix, USA. This tool uses a 24 mm-diameter flash lamp with five lamp drivers capable of emitting broadband light (200-1100 nm) with an intensity of up to 45 kW/cm². The spectral, intensity, and temporal distributions of the light emission from the PLO tool are provided as Figure S1 in the Supporting Information. The beam is extremely uniform, and the variation is less than 5% around the edges. The side of the substrate carrying the PV devices was placed on the processing table with the noncoated side of the carrier facing the flash lamp, and the working distance between the noncoated side of the carrier and the flash lamp was 10 mm. A high intensity light pulse was flashed through the carrier over an interval of 150 μ s with an average pulse fluence of 4.55 \pm 0.04 J/cm². Thermal response at the LAL-polyimide interface during PLO was simulated using the SimPulse software, an interactive photonic pulse thermal response simulation tool that solves a one-dimensional heat conduction model. The essential thermophysical properties of the materials, including optical absorptance, density, thermal conductivity, and heat capacity, are used. The values used in the computations are listed in Table 1. A convective heat flux is defined at all boundaries

Table 1. Material Parameters Used in SimPulse Simulation

material	density (g/cm³)	thermal conductivity $(W/m \cdot K)$	heat capacity (J/kg·°C)
LAL (Ti/W)	19.25	160	134
Eagle XG glass	3.28	1100	1.2
polyimide (from PI2525)	1.42	0.15	1089

using a convective heat transfer coefficient of 15 W m $^{-1}$ °K $^{-1}$ as the sample is typically suspended in air during the PLO process. More information on the governing equations for this 1-D modeling tool and its validation can be found in Guillot *et al.*^{29,30}

Material Characterization. Scanning electron microscopy (SEM) images were obtained using a Zeiss Supra 40 VP SEM operated at an 8 keV accelerating voltage. Samples were electrically grounded to the SEM sample holder with copper tape to prevent charging. Optical transmittance and reflectance spectra were measured in a 2 inch integrating sphere (StellarNet Inc., IC2) using a StellarNet Inc., Blue Wave spectrophotometer with a deuterium-tungsten light source (Analytical Instrument Systems Inc., DT2000). Spectra were analyzed using SpectraWiz spectrometer software (StellarNet Inc.).

PV Device Characterization. Current—voltage characteristics of the PVs were measured with a Keithley 2400 general purpose source meter and a Xe lamp equipped with an A.M. 1.5 filter. Conductive silver paint (SPI Supplies) was applied to make contact between the top contact layer (ITO or AgNW) and the electrical probes.

■ RESULTS AND DISCUSSION

Figure 2a illustrates the PLO process. An intense broad band pulse of light (35 kW/cm², 150 μ s, 200–1100 nm) is provided to the thin LAL, which consists of 200 nm of W/Ti alloy. The LAL converts the incident light pulse into heat and facilitates lift-off of the device layer. In this study, we used PI as the substrate material to support the PV devices. The LAL also prevents direct illumination of the device layer. Figure 2b shows the photographs of an array of CuInSe₂ nanocrystal PVs

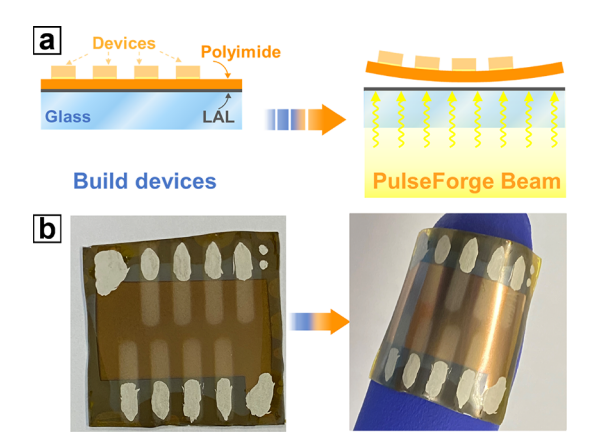


Figure 2. (a) Illustration of the PLO process and the material stack. As shown on the left, PVs are fabricated on a thin layer of PI that has been deposited on the metal LAL on a rigid glass carrier. As shown on the right, the light pulse is delivered through the glass side of the substrate to illuminate the LAL and generate the heat needed to release the PI film carrying the PV devices. (b) Photographs of an array of CuInSe₂ nanocrystal solar cells. The active area of each device is approximately 0.1 cm². The image on the left shows the device layer on the underlying glass support prior to PLO, and on the right, the ultrathin PI-supported solar cells have been released from the substrate and are wrapped around a gloved finger.

before and after the PLO process. The lifted-off PVs are still functional and can be curled, bent, and flexed as shown.

The thermal response of the LAL during the PLO process was simulated using the SimPulse program using typical lift-off pulse conditions (35 kW/cm², 150 μ s) using the optical transmittance T, and reflectance R, of the LAL-coated glass carriers shown in Figure 3. The total light absorbed by the

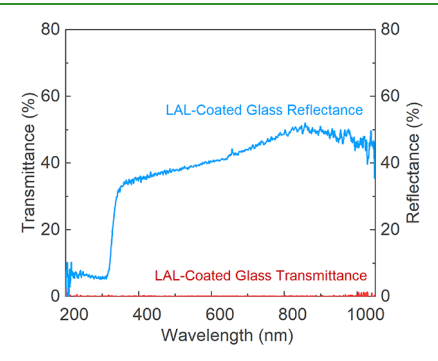


Figure 3. Optical transmittance and reflectance spectra of an LAL-coated glass carrier.

LAL-coated glass during the PLO process is determined by integrating the absorptance A of the LAL over the entire spectral range. The absorptance A is related to T and R as A=100%-T-R. The LAL-coated glass absorbs 55% of the incident light during the PLO process. Note that the transmittance of the LAL is near zero, as needed to prevent light penetration to the devices. Figure 4 shows the temperature increase at the LAL-PI interface calculated using a model of a 20 μ m film of PI on the LAL-coated glass substrate using a 150 μ s light pulse. The temperature at the LAL-PI interface reaches 855 °C in about 200 μ s and then rapidly drops to 350 °C after only 350 μ s. Al-Ajaj and Kareem³² showed by thermal gravimetric analysis (TGA) that polyimide films begin to vaporize at temperatures between 600

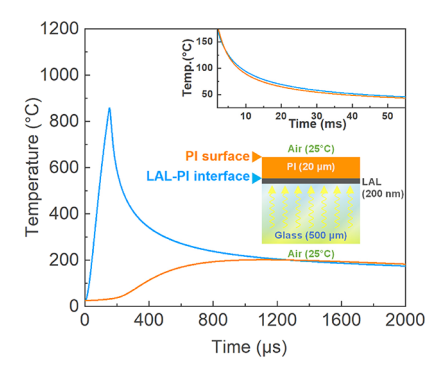


Figure 4. Temperatures of the LAL–PI interface (blue curve) and PI interface (orange curve) calculated using the SimPulse program based on 20 μm of PI on the LAL-coated glass substrate illuminated by a 150 μs pulse at 45 kW/cm² in air at 25 °C. (Inset) The temperatures at the LAL–PI surface (blue curve) and the PI surface (orange curve) drop below 50 °C within 50 ms.

and 700 °C. The temperature at the LAL–PI interface greatly exceeds this during the PLO process, resulting in the release of the PI film and device layer. In this way, PLO is fundamentally similar to the laser lift-off process^{18–20} but with the advantage of large-area illumination.³³

The rapid response of the transient PLO process ensures that devices do not experience exceedingly high temperatures. The model calculations show that the PI surface in contact with the PV devices does not exceed 200 °C, re-equilibrating back to room temperature within 50 ms. Significant heat transfer from the LAL to the PV devices is prevented by the low thermal conductivity of the PI layer (0.146 W/m·K at room temperature),34 and most of the heat generated at the LAL is dissipated through the glass carrier substrate due to its much higher thermal conductivity (1.09 W/m·K at room temperature). The intervening vapor layer (thermal conductivity of 0.0262 W/m·K at room temperature) that is created between the PI and LAL during the release of the device layer (i.e., lift-off) also further reduces heat conduction to the devices. The optical and thermal protection provided by the LAL enables the use of a variety of other polymers as well, including both thermosets and thermoplastics (see the Supporting Information, Figure S4).

The integrity of the different material layers used in the PV devices was examined after PLO. Figure 5a shows the SEM images of a CuInSe₂ nanocrystal layer deposited on Au-coated

PI before and after PLO. There are no distinct cracks or changes in morphology. Figure 5b shows the XRD of the CuInSe₂ nanocrystal layer before and after PLO. There is no loss of chalcopyrite crystal structure and no indication that impurities like CuSe or In₂Se₃ form, which are the typical byproducts of high temperature degradation of CuInSe₂. This provides further confirmation that the devices do not experience high temperatures during PLO. Similar characterization of the CdS and ZnO layers also showed that PLO does not damage these materials (see the Supporting Information, Figure S5).

Although there was no thermal damage to the devices during the PLO process, we found that the transparent conductive oxide (TCO) top contact layer of ITO was too brittle. Figure 6a shows the devices made with ITO top contacts. They have

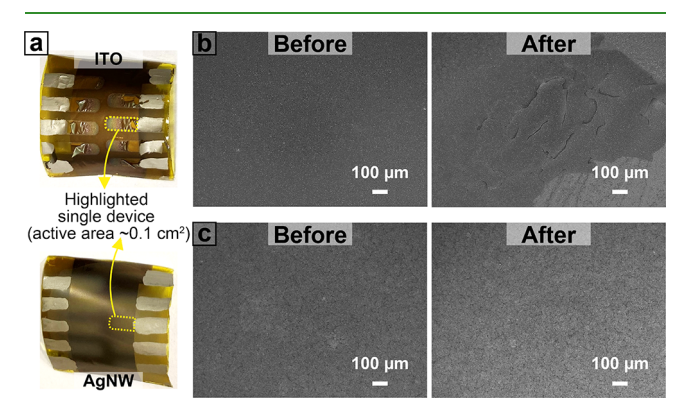


Figure 6. (a) Photographs of devices with ITO top contact cracking after PLO (top) and devices with AgNW top contact intact after PLO (bottom). The active area outlined in yellow of each device is around 0.1 cm². (b) SEM images of an ITO top contact (left) before and (right) after PLO. PLO leads to significant cracking of the ITO layer. (c) SEM images of the spray-coated AgNW film as the top contact before PLO (left) and after PLO (right).

obvious problems with cracking and delamination. The SEM images of the devices after PLO in Figure 6b also reveal significant cracking of the ITO layer. The PVs made with ITO top contacts no longer functioned after PLO (see the Supporting Information Figure S6 for device performance data). We found that the top contact layers of AgNW resolved that problem. AgNW layers can be deposited to form films with optical transparency and electrical conductivity com-

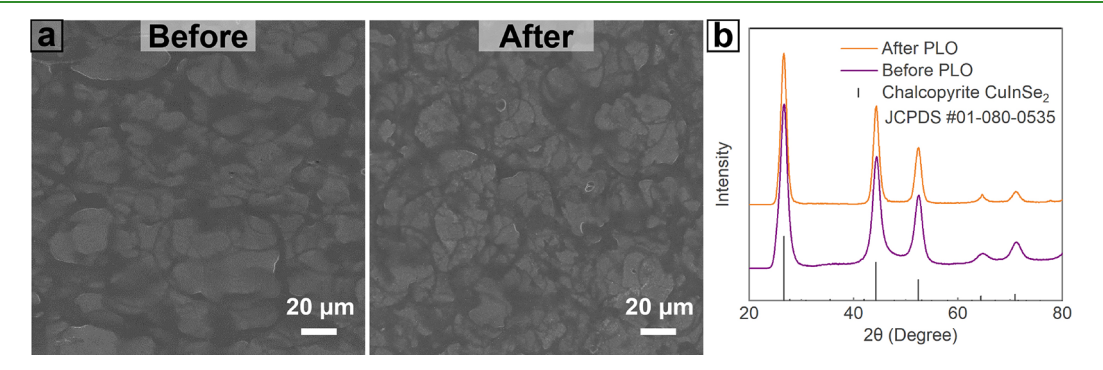


Figure 5. (a) SEM images of a CuInSe₂ nanocrystal film spray-deposited on PI before PLO (left), showing the typical island-like grain morphology from spray-coating, and after PLO (right), the morphology was retained without any crack formation. (b) XRD patterns of a CuInSe₂ nanocrystal film spray-coated on polyimide before and after PLO. The reference XRD peaks provided as gray drop lines correspond to JCPDS no. 01-080-0535 for chalcopyrite CuInSe₂.

parable to ITO,³⁷ with an added advantage of being able to be deposited from solution under ambient conditions. As shown in the bottom photograph in Figure 6A, the AgNW film does not crack after PLO. The SEM images of a spray-deposited AgNW film shown in Figure 6c also show no signs of crack formation in the AgNW layer after PLO.

PVs made with AgNW top contacts remain functional after PLO. The average power conversion efficiency (PCE) of the devices decreased slightly from 1.8 to 1.6%, as shown in Figure 7a, but the AgNW top contacts solve the problem of top

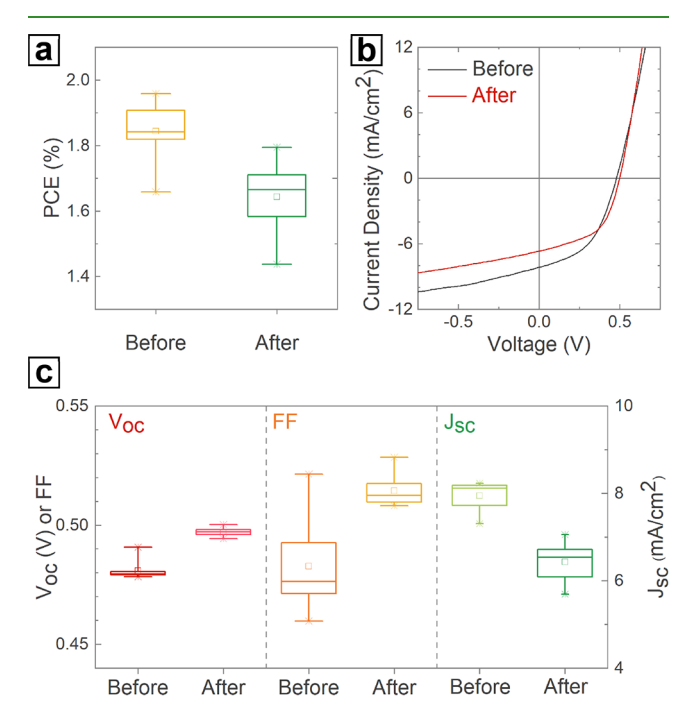


Figure 7. (a) Box plot of the PCE of devices fabricated with AgNW top contacts on polyimide substrates before and after PLO. The box plot denotes median (center line), mean value (dot), 25th (bottom edge of the box), 75th (top edge of the box), 95th (upper whisker), and 5th (lower whisker) percentiles. The sample size in each column is eight devices. (b) J-V curve of the best device from the sample group. (c) Performance parameter (V_{oc} , J_{sc} , and FF) box plots before and after PLO.

contact cracking experienced with ITO. Figure 7b shows the current-voltage response of a device before and after PLO. Figure 7c shows the device statistics. After PLO, there are no changes in open-circuit voltage (V_{oc}) and fill factor (FF), but the short-circuit current (I_{sc}) does decrease slightly. Devices made on soda-lime glass using the same fabrication process and then tested at the same time as the devices made on PI also showed a similar J_{sc} drop (Figure S6 in the Supporting Information). The control devices made on soda-lime glass were not exposed to intense beam of light from the PulseForge tool, so we attribute the slight loss of short-circuit current and decline in performance to material and device aging and not the PLO process.

The PV device performance was improved by combining both AgNW and ITO as the top contact layer. The AgNW top contacts eliminated cracking during PLO, but the AgNW top contacts yielded devices with slightly reduced performance, with PCEs of around 2.0% compared to 2.5% when ITO is used. The spray-deposited AgNW films exhibited optical absorbance comparable to sputter-deposited ITO and were

even more electrically conductive (sheet resistance of ITO is ~19 Ω /sq while AgNW exhibits ~5 Ω /sq); however, the electrical contact of the nanowire network with the underlying ZnO layer is not as good and the higher work function 38,39 of Ag leads to a lower carrier collection efficiency and PCE. To seek an optimal ratio for flexibility and performance, a series of combinations of these two materials were implemented for the solar cell top contact. As Table 2 shows, the different top

Table 2. Coating Conditions and PCE Results of Group 1, 2, and 3 Devices

device group no.	no. of AgNW coating cycles	ITO thickness (nm)	% of devices retaining near original PCE after PLO
group 1	12	200	5%
group 2	15	120	33%
group 3	18	50	100%

contact compositions in group 1, group 2, and group 3 devices were controlled by the thickness of the ITO film and the number of AgNW spray-coating cycles. With lowering the ITO film thickness from 200 to 120 nm, and eventually to 50 nm, the yield of functional devices, which exhibited near original PCE after PLO, increased from less than 5% to about 33% and then 100%, respectively. As shown in the after-PLO pictures (Figure 8a-c), group 1 devices clearly cracked, group 2 still exhibited minor cracks, while group 3 devices, with 50 nm ITO and 18 coating cycles of AgNW that correspond to a film thickness of 320 nm, were all free of morphology damages. Also, they showed comparable PCE before and after PLO, similarly with no change in $V_{\rm oc}$ or FF but slightly lower $J_{\rm sc}$ values (Figure 8d-f). For every group of devices, a control sample was made on soda-lime glass under the same conditions for comparison. The PCE of the control sample for group 3 devices also decreased slightly over time at about the same rate as the devices processed by PLO due to J_{sc} changes (Figure S8 in the Supporting Information).

Table 3 summarizes the PCE obtained from the devices made with the three different top contacts of ITO, AgNW, and ITO with AgNW. The cracking of the ITO top contacts during lift-off resulted in no working devices after PLO. The solar cells on PI fabricated with the combination of AgNW and ITO demonstrated the highest PCE, with a champion PCE of 2.8 and 2.2% before and after PLO. Overall, these results demonstrate that the PLO process can aid in fabricating lightweight, ultrathin ($<20 \mu m$) solar cells that could be attractive for space and stratospheric applications. Further, this process, as demonstrated, also enables monolithic device fabrication on the top of polymeric films, not requiring transferring the completed devices to foreign substrates after lift-off, which is a typical step in other lift-off mechanisms. 8-20

CONCLUSIONS

Fabrication of ultrathin solar cells less than 20 μ m thick using the PLO process was demonstrated. The PLO process involves separating thin and flexible, device-carrying polymeric films from a rigid carrier by irradiating an LAL with high-intensity pulsed light. The LAL-PI interface reaches 855 °C during the PLO process, which promotes lift-off of the PI layer. The devices do not experience these extreme temperatures because the LAL blocks light penetration to the devices and the heating generated by the rapid light pulse is quickly dissipated through

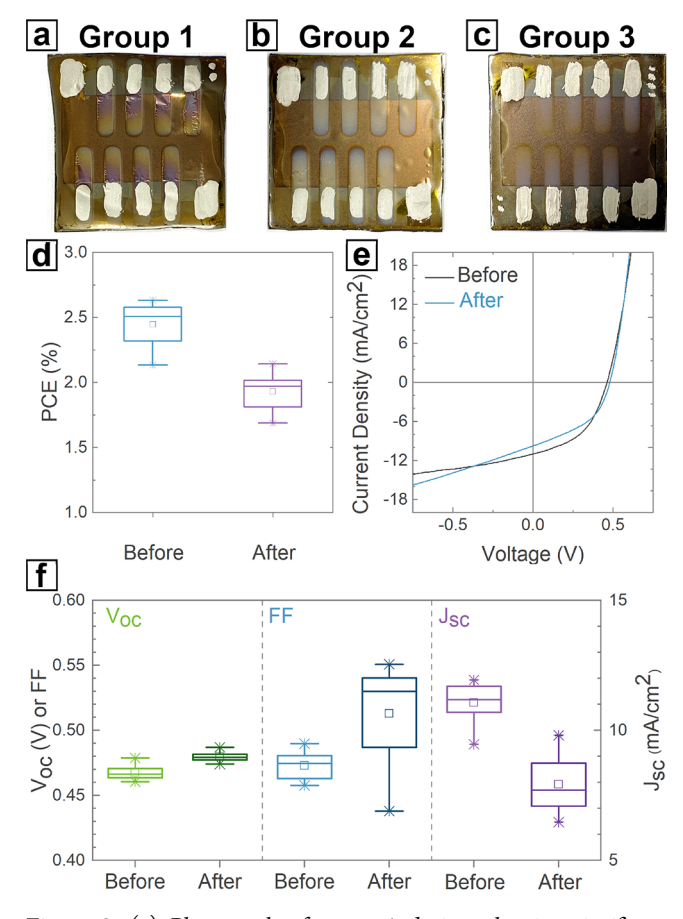


Figure 8. (a) Photograph of group 1 devices showing significant cracking of ITO after PLO. (b) Photograph of group 2 devices showing minor cracking after PLO. (c) Photograph of group 3 devices all free of morphology damages after PLO. (d) PCE statistics box plot of group 3 devices before and after PLO. The box plot denotes median (center line), mean value (dot), 25th (bottom edge of the box), 75th (top edge of the box), 95th (upper whisker), and 5th (lower whisker) percentiles. The sample size in each column is eight devices. (e) J-V curve of the best device from group 3. (f) Performance parameter box plots of group 3 devices before and after PLO.

Table 3. Summary of Champion PCE for Devices with **Different Top Contact Compositions**

top contact	champion PCE before PLO	champion PCE after PLO	
ITO	2.57%	0	
AgNW	1.96%	1.79%	
AgNW and ITO	2.84%	2.20%	

the glass substrate. SEM and XRD data all confirmed that the materials in the device layers maintain their integrity during the PLO process, with no observable changes in morphological or structural attributes of the solar cells. The only modification required was a change in the top contact material from ITO to AgNW or a combination of ITO and AgNW. The typical ITO top contacts were found to be too brittle and prone to cracking during the lift-off process to be used effectively with PLO. With the improvement in mechanical durability of the top contacts, PV devices could be lifted-off without significant degradation in PCE. CuInSe₂ nanocrystal solar cells on the flexible PI substrate with a champion efficiency of 2.2% were fabricated using a top contact layer of thin ITO and AgNW.

The PLO process is amenable to the use of other types of polymer substrates as well. This work exemplifies how solution-processable materials and processes can be coupled with PLO to achieve new pathways to fabricate low-cost, lightweight, and ultrathin electronic and optoelectronic devices.

ASSOCIATED CONTENT

Supporting Information

The Supporting Information is available free of charge at https://pubs.acs.org/doi/10.1021/acsami.1c12382.

Spectral and intensity distribution of light emission from a PulseForge lamp and temporal distribution of a typical light pulse used in the PLO process; photographs of three different polymer films delaminated from glass substrates using the PLO process; SEM images of CdS and ZnO layers used in CuInSe2 nanocrystal PV device structures before and after PLO; and additional PCE data of devices with ITO top contacts made on PI substrates before and after PLO, control devices made on soda-lime glass with AgNW top contacts, and control devices made on soda-lime glass with AgNW-ITO-mixed top contact (PDF)

AUTHOR INFORMATION

Corresponding Author

Brian A. Korgel - McKetta Department of Chemical Engineering and Texas Materials Institute, The University of Texas at Austin, Austin, Texas 78712, United States; orcid.org/0000-0001-6242-7526; Email: korgel@ che.utexas.edu

Authors

Wen Liu - McKetta Department of Chemical Engineering and Texas Materials Institute, The University of Texas at Austin, Austin, Texas 78712, United States; o orcid.org/0000-0001-8379-0981

Vikram S. Turkani – NovaCentrix, Austin, Texas 78728, United States

Vahid Akhavan - Nova Centrix, Austin, Texas 78728, United

Complete contact information is available at: https://pubs.acs.org/10.1021/acsami.1c12382

Notes

The authors declare the following competing financial interest(s): In accordance with ethical obligations as researchers, the authors acknowledge financial interest by Vikram S. Turkani and Vahid Akhavan as employees of NovaCentrix in the outcome of this research.

ACKNOWLEDGMENTS

We acknowledge funding of this research by the Robert A. Welch Foundation (grant no. F-1464) and the Industry/ University Cooperative Research Center (IUCRC) for Next Generation Photovoltaics (IIP-1822206). We thank John Passiak, Rob J. Hendriks, and Holst Centre, Netherlands, for assistance with temporal distribution and lamp uniformity measurements. We also thank Dr. Kurt A. Schroder for helpful discussions about the PLO process.

REFERENCES

- (1) Sharma, S.; Jain, K. K.; Sharma, A. Solar Cells: In Research and Applications—A Review. *Mater. Sci. Appl.* **2015**, *06*, 1145–1155.
- (2) Pagliaro, M.; Ciriminna, R.; Palmisano, G. Flexible Solar Cells. ChemSusChem 2008, 1, 880-891.
- (3) Massiot, I.; Cattoni, A.; Collin, S. Progress and Prospects for Ultrathin Solar Cells. *Nat. Energy* **2020**, *5*, 959–972.
- (4) Voggu, V. R.; Sham, J.; Pfeffer, S.; Pate, J.; Fillip, L.; Harvey, T. B.; Brown, R. M., Jr.; Korgel, B. A. Flexible CuInSe₂ Nanocrystal Solar Cells on Paper. *ACS Energy Lett.* **2017**, *2*, 574–581.
- (5) Ramanujam, J.; Bishop, D. M.; Todorov, T. K.; Gunawan, O.; Rath, J.; Nekovei, R.; Artegiani, E.; Romeo, A. Flexible CIGS, CdTe and a-Si:H Based Thin Film Solar Cells: A Review. *Prog. Mater. Sci.* **2020**, *110*, 100619–100620.
- (6) Reinhard, P.; Chirilă, A.; Blösch, P.; Pianezzi, F.; Nishiwaki, S.; Buecheler, S.; Tiwari, A. N. Review of Progress toward 20% Efficiency Flexible CIGS Solar Cells and Manufacturing Issues of Solar Modules. *IEEE J. Photovoltaics* **2013**, *3*, 572–580.
- (7) Wang, Y. C.; Wu, T. T.; Chueh, Y. L. A Critical Review on Flexible Cu(In, Ga)Se₂ (CIGS) Solar Cells. *Mater. Chem. Phys.* **2019**, 234, 329–344.
- (8) Fleutot, B.; Lincot, D.; Jubault, M.; Li Kao, Z. J.; Naghavi, N.; Guillemoles, J. F.; Donsanti, F. GaSe Formation at the Cu(In,Ga)Se₂/Mo Interface-A Novel Approach for Flexible Solar Cells by Easy Mechanical Lift-Off. *Adv. Mater. Interfaces* **2014**, *1*, 1400044–1400012.
- (9) Minemoto, T.; Abe, Y.; Anegawa, T.; Osada, S.; Takakura, H. Lift-off Process for Flexible Cu(In,Ga)Se₂ Solar Cells. *Jpn. J. Appl. Phys.* **2010**, 49, 1–3.
- (10) Nishimura, T.; Hamada, N.; Chantana, J.; Mavlonov, A.; Kawano, Y.; Masuda, T.; Minemoto, T. Application of Two-Dimensional MoSe₂ Atomic Layers to the Lift-Off Process for Producing Light-Weight and Flexible Bifacial Cu(In,Ga)Se₂ Solar Cells. ACS Appl. Energy Mater. 2020, 3, 9504–9508.
- (11) Anegawa, T.; Oda, Y.; Minemoto, T.; Takakura, H. Comparison of Lift-off Processes and Rear-Surface Characterization of Cu(In,Ga)Se₂ Thin Films for Solar Cells. *J. Cryst. Growth* **2009**, 311, 742–745.
- (12) Marrón, D. F.; Meeder, A.; Sadewasser, S.; Würz, R.; Kaufmann, C. A.; Glatzel, T.; Schedel-Niedrig, T.; Lux-Steiner, M. C. Lift-off Process and Rear-Side Characterization of CuGaSe₂ Chalcopyrite Thin Films and Solar Cells. *J. Appl. Phys.* **2005**, 97, No. 094915.
- (13) Osada, S.; Abe, Y.; Anegawa, T.; Minemoto, T.; Takakura, H. Cu(In,Ga)Se₂ Solar Cells with Superstrate Structure Using Lift-off Process. *Sol. Energy Mater. Sol. Cells* **2011**, *95*, 223–226.
- (14) Tiwari, A. N.; Krejci, M.; Haug, F. J.; Zogg, H. 12.8% Efficiency Cu(In,Ga)Se₂ Solar Cell on a Flexible Polymer Sheet. *Prog. Photovolt.:* Res. Appl. 1999, 7, 393–397.
- (15) Bauhuis, G. J.; Mulder, P.; Haverkamp, E. J.; Huijben, J. C. C. M.; Schermer, J. J. 26.1% Thin-Film GaAs Solar Cell Using Epitaxial Lift-Off. Sol. Energy Mater. Sol.Cells 2009, 93, 1488–1491.
- (16) Yoon, J.; Jo, S.; Chun, I. S.; Jung, I.; Kim, H. S.; Meitl, M.; Menard, E.; Li, X.; Coleman, J. J.; Paik, U.; Rogers, J. A. GaAs Photovoltaics and Optoelectronics Using Releasable Multilayer Epitaxial Assemblies. *Nature* **2010**, *465*, 329–333.
- (17) Konagai, M.; Sugimoto, M.; Takahashi, K. Hight Efficiency GaAs Thin Film Solar Cells by Peeled Film Technology. *J. Cryst. Growth* **1978**, 45, 277–280.
- (18) Gecys, P.; Markauskas, E.; Gedvilas, M.; Raciukaitis, G.; Repins, I.; Beall, C. Ultrashort Pulsed Laser Induced Material Lift-off Processing of CZTSe Thin-Film Solar Cells. *Sol. Energy* **2014**, *102*, 82–90.
- (19) Lee, S. I.; Jang, S. H.; Han, Y. J.; Lee, J. Y.; Choi, J.; Cho, K. H. Xenon Flash Lamp Lift-off Technology without Laser for Flexible Electronics. *Micromachines* **2020**, *11*, 1–11.
- (20) Dang, B.; Andry, P.; Tsang, C.; Maria, J.; Polastre, R.; Trzcinski, R.; Prabhakar, A.; Knickerbocker, J. CMOS Compatible Thin Wafer Processing Using Temporary Mechanical Wafer, Adhesive and Laser

- Release of Thin Chips/Wafers for 3D Integration. 2010 Proceedings 60th Electronic Components and Technology Conference (ECTC); IEEE: 2010. 1393–1398.
- (21) Khan, S. A.; Rahman, A. Efficiency of Thin Film Photovoltaic Paint: A Brief Review. *Int. J. Recent Technol. Eng.* **2019**, *7*, 163–169. (22) Townsend, T. K.; Foos, E. E. Fully Solution Processed All Inorganic Nanocrystal Solar Cells. *Phys. Chem. Chem. Phys.* **2014**, *16*, 16458–16464.
- (23) Yuan, J.; Bi, C.; Wang, S.; Guo, R.; Shen, T.; Zhang, L.; Tian, J. Spray-Coated Colloidal Perovskite Quantum Dot Films for Highly Efficient Solar Cells. *Adv. Funct. Mater.* **2019**, 29, 1906615.
- (24) Choi, H.; Lee, J. G.; Mai, X. D.; Beard, M. C.; Yoon, S. S.; Jeong, S. Supersonically Spray-Coated Colloidal Quantum Dot Ink Solar Cells. Sci. Rep. 2017, 7, 622.
- (25) Akhavan, V. A.; Panthani, M. G.; Goodfellow, B. W.; Reid, D. K.; Korgel, B. A. Thickness-Limited Performance of CuInSe₂ Nanocrystal Photovoltaic Devices. *Opt. Express* **2010**, *18*, A411.
- (26) Akhavan, V. A.; Goodfellow, B. W.; Panthani, M. G.; Steinhagen, C.; Harvey, T. B.; Stolle, C. J.; Korgel, B. A. Colloidal CIGS and CZTS Nanocrystals: A Precursor Route to Printed Photovoltaics. *J. Solid State Chem.* **2012**, *189*, 2–12.
- (27) Panthani, M. G.; Stolle, C. J.; Reid, D. K.; Rhee, D. J.; Harvey, T. B.; Akhavan, V. A.; Yu, Y.; Korgel, B. A. CuInSe₂ Quantum Dot Solar Cells with High Open-Circuit Voltage. *J. Phys. Chem. Lett.* **2013**, 4, 2030–2034.
- (28) McCandless, B. E.; Shafarman, W. N. Chemical Surface Deposition of Ultra-Thin Semiconductors. U.S. Patent 6,537,845 B1, 2003.
- (29) Guillot, M. J.; Schroder, K. A.; McCool, S. C. Simulating the Thermal Response of Thin Films During Photonic Curing. ASME International Mechanical Engineering Congress and Exposition; American Society of Mechanical Engineers: 2012, 1–9.
- (30) NovaCentrix SimPulse ® Photonic Curing Simulation https://www.novacentrix.com/sites/default/files/pdf/NovaCentrix_SimPulse brochure.pdf (accessed 2021-06-17).
- (31) Schroder, K. A.; McCool, S. C.; Furlan, W. F. Broadcast Photonic Curing of Metallic Nanopartiele Films. 2006 NSTI Nanotechnol. Conf. Trade Show NSTI Nanotech 2006 Tech. Proc.; 2006, 3, 198–201.
- (32) Al-Ajaj, I. A.; Kareem, A. A. Synthesis and Characterization of Polyimide Thin Films Obtained by Thermal Evaporation and Solid State Reaction. *Mater. Sci. Pol.* **2016**, *34*, 132–136.
- (33) Turkani, V. PulseForge Lift-Off: A Flashlamp Lift-Off Process; https://www.novacentrix.com/sites/default/files/pdf/2020-04-02_PulseForge Liftoff QA v7.pdf (accessed 2020-07-16).
- (34) HD MicroSystems *Product Bulletin*; PI 2525, PI 2555 & PI 2574 www.hdmicrosystems.com (accessed 2020-06-04).
- (35) Scragg, J. J.; Dale, P. J.; Colombara, D.; Peter, L. M. Thermodynamic Aspects of the Synthesis of Thin-Film Materials for Solar Cells. *ChemPhysChem* **2012**, *13*, 3035–3046.
- (36) Deng, W.; Yan, Z.; Deng, P.; Wang, Y.; Fang, Y.; Sun, M.; Su, Y. Phase Composition of CuInSe₂ in Different Annealing Process. *Mater. Sci. Semicond. Process.* **2014**, *26*, 419–424.
- (37) Hu, L.; Kim, H. S.; Lee, J. Y.; Peumans, P.; Cui, Y. Scalable Coating and Properties of Transparent, Flexible, Silver Nanowire Electrodes. *ACS Nano* **2010**, *4*, 2955–2963.
- (38) Leem, D. S.; Edwards, A.; Faist, M.; Nelson, J.; Bradley, D. D. C.; De Mello, J. C. Efficient Organic Solar Cells with Solution-Processed Silver Nanowire Electrodes. *Adv. Mater.* **2011**, 23, 4371–4375.
- (39) Park, Y.; Choong, V.; Gao, Y.; Hsieh, B. R.; Tang, C. W. Work Function of Indium Tin Oxide Transparent Conductor Measured by Photoelectron Spectroscopy. *Appl. Phys. Lett.* **1996**, *68*, 2699–2701.